

Red-light-driven Photocatalytic hydrogen evolution using a ruthenium quaterpyridine complex

E. Rousset,^{a,b} D. Chartrand,^a I. Ciofini,^c V. Marvaud,^{b*} and G. S. Hanan,^{a*}

SUPPORTING INFORMATION

Contents :

<i>S.I.-1 Instrumentation details:</i>	2
<i>S.I.-2 Experimental Part:</i>	3
<i>S.I.-3 Crystallography additional information:</i>	4
S.I.-3a [Ru(qpy) ₃ (Cl) ₂]	4
S.I.-3b [Ru(qpy) ₃ (PF ₆) ₂]	7
<i>S.I.-4 Computational Details:</i>	10
<i>S.I.-5 Photocatalysed hydrogen production:</i>	17
<i>References</i>	19

S.I.-1 Instrumentation details:

Nuclear Magnetic Resonance (NMR) spectra were recorded in deuterated solvents at room temperature on a Bruker AV400 for ^1H -NMR (400 MHz) and ^{13}C -NMR (101 MHz). Chemical shifts are reported in parts per million (ppm) relative to residual protons and carbon resonances of the solvent. All coupling constants are given in Hertz (Hz).

Absorption spectra were recorded using a Cary 500i UV-Vis-NIR spectrophotometer in spectroscopic grade acetonitrile. Emission spectra were recorded using a Cary Eclipse 300 fluorimeter. The excitation wavelengths for the emission spectra were determined using the absorption maxima of the metal-ligand charge transfer transition band. Photophysical measurements were done in air-equilibrated and degassed spectroscopic grade acetonitrile, using a quartz cell. The quantum yield of interest is calculated using the dilute method^{S1} using two different references: solutions of $[\text{Ru}(\text{bpy})_3(\text{PF}_6)_2]$ degassed and aerated, considered according to the value described in literature at 0.095 ± 0.003 et 0.018 ± 0.003 respectively.^{S2} Excited state lifetimes were determined on an Edinburgh OB 900 single-photon-counting spectrometer, employing a Hamamatsu PLP2 laser diode as pulse (wavelength output, 408 nm; pulse width, 59 ps).

Electrochemical measurements were carried out in argon-purged spectroscopic grade acetonitrile at room temperature with a BAS CV50W multipurpose potentiostat. The working electrode was a glassy carbon electrode (2 mm in diameter), the counter electrode was a Pt wire, and the pseudo-reference electrode was a silver wire. The reference was set using an internal 1.0 mM ferrocene/ferrocinium sample with its redox couple adjusted to 395 mV vs SCE in acetonitrile. The concentration of the compound was around 10^{-3} M. Tetrabutylammonium hexafluorophosphate was used as supporting electrolyte, and its concentration was 0.10 M.

S.I.-2 Experimental Part:

Synthesis of the ligand quaterpyridine was adapted from the one reported in the literature.^{S3} Ru(DMSO)₄Cl₂ was synthesised as reported in the literature.^{S4} All chemicals were purchased from commercial suppliers and used without further purification. The properties of the qpy ligand^{S3} and [Ru(qpy)₃(PF₆)₂] complex^{S5} were consistent with previously reported data.

4,4':2',2":4",4'''-quaterpyridine: 4,4'-bipyridine (10 g, 32 mmol) and palladium on charcoal (2 g, 10 %) were heated at 250°C for two days in a solvothermal Teflon bomb. The resulting solid was ground and extracted with a Soxhlet extractor using dichloromethane giving a first fraction. The palladium residue was then washed with hot DMF, the latter being removed under vacuum to give a second crop. The two fractions are reunited and purified by chromatography on silica gel using a gradient of DCM/MeOH (from 99:1 to 90:10) to afford an off-white powder (4.04 g, Y=41%). ¹H NMR (400 MHz, CD₂Cl₂) δ = 8.90-8.83 (m, 4H), 8.83-8.76 (m, 4H), 7.78-7.71 (m, 4H), 7.68 (dd, *J* = 5, 2 Hz, 2H). IR (KBr pellets, cm⁻¹) : 1586, 1533, 1463, 1364, 807, 616, 508.

[Ru(qpy)₃(PF₆)₂]: Ru(DMSO)₄Cl₂ (20 mg, 4.12•10⁻⁵ mol) and 4,4':2',2":4",4'''-quaterpyridine (38.4 mg, 1.25•10⁻⁴ mol) were dissolved in ethylene glycol (20 mL). The resulting suspension was heated at 240°C for 15 minutes using microwave irradiation (*P*_{max} = 400 W). After cooling the mixture, water was added followed by a saturated aqueous solution of potassium hexafluorophosphate yielding a red precipitate, which was filtered on celite and washed with water (2 x 10 mL) and diethylether (2 x 10 mL). The desired product was dissolved in acetonitrile, concentrated under vacuum and was precipitated with diethylether to afford a red powder (107 mg, Y=97%). ¹H NMR (400 MHz, CD₃CN) δ = 9.01 (dd, *J* = 2, 0.5 Hz, 2H), 8.86 - 8.79 (m, 4H), 7.99 (dd, *J* = 6, 0.5 Hz, 2H), 7.90 - 7.83 (m, 4H), 7.78 (dd, *J* = 6, 2 Hz, 2H). ¹³C NMR (100 MHz, CD₃CN) δ = 158.6, 153.4, 151.7, 148.2, 144.3, 126.5, 123.7, 122.8 . IR (KBr pellets, cm⁻¹) : 1598, 1532, 1472, 1405, 841, 814, 628, 557.

S.I.-3 Crystallography additional information:

S.I.-3a [Ru(qpy)₃(Cl)₂]

Table S1: Crystallographic information of complex [Ru(qpy)₃]Cl₂

Compound	[Ru(qpy) ₃]Cl ₂
CCDC Number	1046675
Formula	(C ₆₀ H ₄₂ N ₁₂ Ru ₁) 2(Cl) 5(H ₂ O)
M_w (g.mol ⁻¹) : d _{calcd} (g.cm ⁻³)	1192.89 : 0.835
T (K)	100(2)
F(000)	2416
Crystal System	Cubic
Space Group	P4 ₁ 32
Unit Cell	
<i>a</i> (Å)	21.1118(3)
<i>b</i> (Å)	21.1118(3)
<i>c</i> (Å)	21.1118(3)
α (°)	90.00
β (°)	90.00
γ (°)	90.00
<i>V</i> (Å ³) : Z	9409.7(2) : 4
θ_{range} (°) : completeness	2.96-53 : 99.7%
R _{flc} :collec./indep. : R _{int}	94438/3021: 9.78%
<i>m</i> (mm ⁻¹)	2.168
R1 ^a : wR2 ^b : GoF ^c	0.0669 : 0.2055 : 1.172
max/min residual electron density (e.Å ⁻³)	0.515 / -0.728
Flack parameter	0.029(8)

^a R1 defined as $\sum |F_0| - |F_c| / \sum |F_0|$ ^b wR2 defined as $\{\sum [w(F_0^2 - F_c^2)^2] / [\sum w(F_0^2)^2]\}^{1/2}$ ^c R1 based on observed reflections with [I > 2s(I)]; wR2 and GoF based on all data.

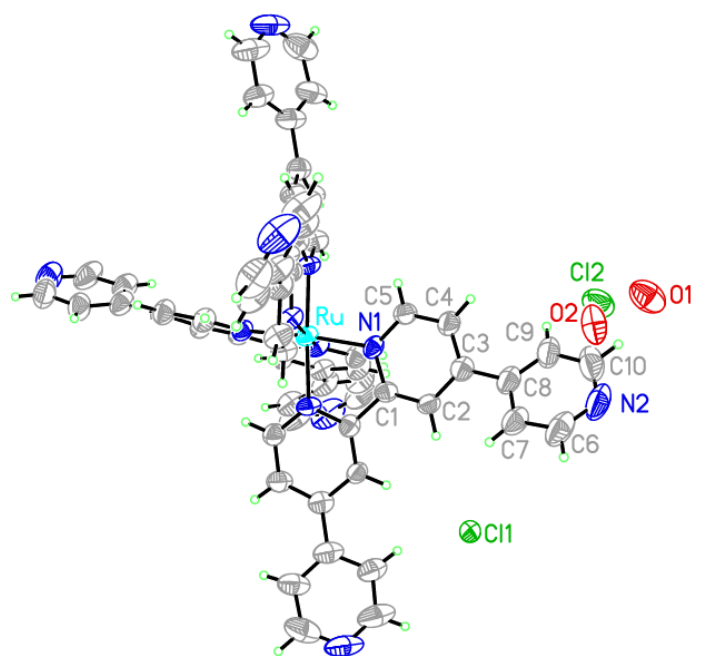


Figure S1: ORTEP view of the X-ray crystal structure of $[Ru(\text{qpy})_3]\text{Cl}_2$ with the labeling scheme (thermal ellipsoids are drawn at 50% probability).

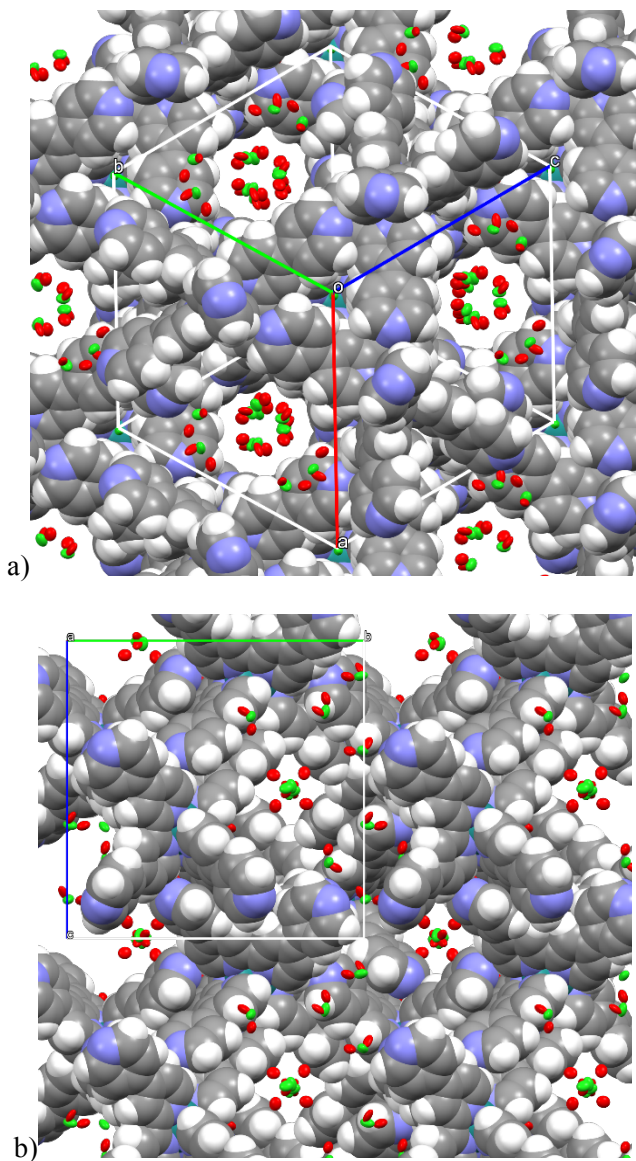


Figure S2: Packing of $[Ru(qpy)_3]Cl_2$ showing the channels along a) the long diagonal of the cubic cell; b) the axes of the cell. (Spacefill view for the main molecule, 50% probability displacement ellipsoids for anions and modeled water molecules).

S.I.-3b [Ru(qpy)₃(PF₆)₂]

Table S2: Crystallographic information of complex [Ru(qpy)₃](PF₆)₂

Compound	[Ru(qpy) ₃](PF ₆) ₂
CCDC Number	1046674
Formula	(C ₆₀ H ₄₂ N ₁₂ Ru ₁) 2(PF ₆) 2(CH ₃ CN) (C ₄ H ₉ O)
M_w (g.mol ⁻¹) : d _{calcd} (g.cm ⁻³)	1 476.84 : 1.231
T (K)	100(2)
F(000)	4517
Crystal System	Trigonal
Space Group	R-3
Unit Cell	
<i>a</i> (Å)	17.6408(12)
<i>b</i> (Å)	17.6408(12)
<i>c</i> (Å)	44.355(3)
α (°)	90.00
β (°)	90.00
γ (°)	120.00
V (Å ³) : Z	11954.0(19) : 6
θ_{range} (°) : completeness	2.600-53.594 : 99.8%
R _{flc} :collec./indep. : R _{int}	99995/4875: 7.74%
<i>m</i> (mm ⁻¹)	1.721
R1 ^a : wR2 ^b : GoF ^c	0.0885 : 0.2708 : 1.113
max/min residual electron density (e.Å ⁻³)	2.035 / -1.120
Flack parameter	n/a

^a R1 defined as $\Sigma |F_0| - |F_c| / \Sigma |F_0|$ ^b wR2 defined as $\{\Sigma[w(F_0^2 - F_c^2)^2] / [w(F_0^2)^2]\}^{1/2}$ ^c R1 based on observed reflections with [I > 2s(I)]; wR2 and GoF based on all data

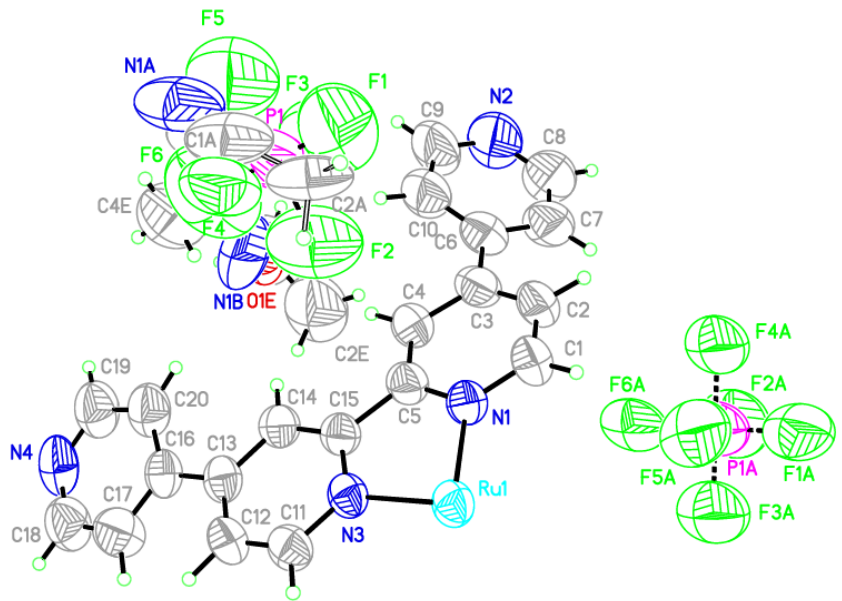


Figure S3 : ORTEP views of the asymmetric unit of X-ray crystal structure of $[Ru(qpy)_3][PF_6]_2$ with the labeling scheme (thermal ellipsoids are drawn at 50% probability).

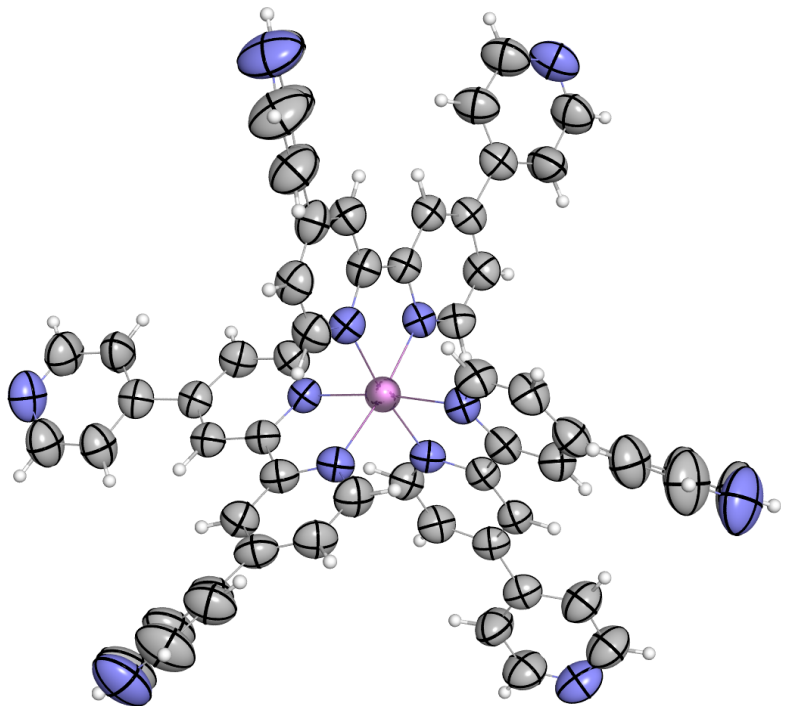


Figure S4: ORTEP view of the X-ray crystal structure of $[Ru(qpy)_3][PF_6]_2$ (thermal ellipsoids are drawn at 50% probability, counter ions and solvent molecules are removed for clarity).

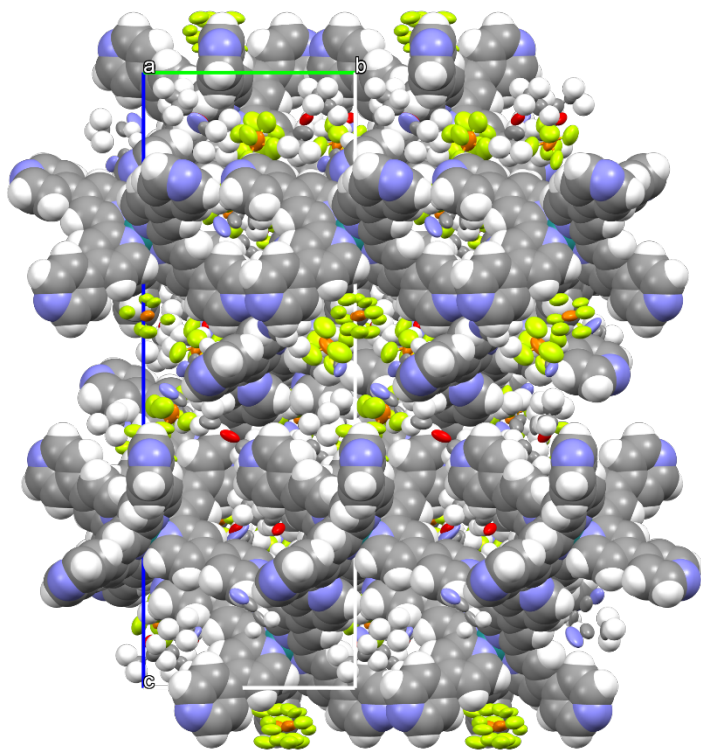


Figure S5 : Packing of $[Ru(qpy)_3][PF_6]_2$ showing along a axis. (Spacefill view for the main molecule, 50% probability displacement ellipsoids for anions and modeled solvents).

S.I.-4 Computational Details:

All calculations were performed using Gaussian 09.^{S6} The geometry of the compound was optimised at the density functional theory (DFT) level with the hybrid PBE0 functional.^{S7} The basis set used was LanL2DZ^{S8} and corresponding pseudopotential was used. Solvent (MeCN) was modelled by a conductor-like polarisable continuum model (cpcm).^{S9} No imaginary frequencies were observed for the optimised geometry. Atoms coordinates are available on Table S3.

Table S3: Atoms coordinates of $[Ru(qpy)_3]^{2+}$ (Å)

Label	Atom	X	Y	Z				
1	C	0.4439260	2.8725770	0.5794830	58	C	3.1463540	6.3868870
2	C	2.2627620	-1.8123270	0.5826480	59	C	7.0680020	-4.4718410
3	C	-2.2525090	-1.8406740	-0.5815060	60	C	-3.1936670	6.3735860
4	C	-0.4670130	2.8711090	-0.5842270	61	H	4.0246960	-3.0287470
5	C	2.7094030	-1.0311100	-0.5898520	62	H	4.6550800	-1.9272710
6	C	-2.7092030	-1.0565400	0.5850080	63	H	-3.9933000	-3.0910440
7	C	3.0338420	-2.8101630	1.1974430	64	H	-4.6498330	-1.9639170
8	C	3.9618980	-1.1870050	-1.2028810	65	H	0.6405160	5.0065420
9	C	-3.0081310	-2.8569350	-1.1855110	66	H	-0.6705490	5.0047150
10	C	-3.9627320	-1.2171030	1.1942120	67	H	2.8077700	2.5257370
11	C	0.9395660	4.0375110	1.1844340	68	H	0.7979700	-3.6734150
12	C	-0.9655120	4.0345500	-1.1896270	69	H	-3.5956080	1.1609220
13	C	1.8032900	3.9583950	2.2967340	70	H	-0.7676910	-3.6956370
14	C	2.5410090	-3.5124310	2.3172830	71	H	-2.8318920	2.5181090
15	C	-4.3268760	-0.4319620	2.3080710	72	H	3.5682880	1.1740140
16	C	-2.5069180	-3.5586220	-2.3019950	73	H	1.8635270	0.5443890
17	C	4.3162760	-0.4060130	-2.3229770	74	H	-0.4615080	-1.8856710
18	C	-1.8296900	3.9528830	-2.3015510	75	H	-1.4126730	1.3482660
19	C	2.1352350	2.6666770	2.7665990	76	H	0.4661680	-1.8804740
20	C	1.2522340	-3.1632460	2.7830620	77	H	-1.8801410	0.5392930
21	C	-3.3791370	0.5083680	2.7738140	78	H	1.3873600	1.3489340
22	C	-1.2268580	-3.1891130	-2.7759470	79	H	5.7072120	-6.9790740
23	C	-2.1588900	2.6604020	-2.7709430	80	H	-8.9187240	-1.4129730
24	C	3.3601330	0.5249610	-2.7904050	81	H	-5.6080300	-7.0835080
25	C	1.6153970	1.5389880	2.1274530	82	H	3.2742300	8.4167400
26	C	0.5263430	-2.1614580	2.1353410	83	H	8.9110320	-1.3694210
27	C	-0.5153980	-2.1710050	-2.1374960	84	H	-3.3112660	8.4078620
28	C	-1.6352150	1.5340740	-2.1324070	85	H	4.3957000	-5.2427460
29	C	2.1276120	0.6405170	-2.1439860	86	H	-6.7538030	-1.1625370
30	C	-2.1460710	0.6305130	2.1295320	87	H	-4.3283100	-5.3089220
31	C	5.0005890	-6.3587310	2.9197340	88	H	2.3921610	6.4155120
32	C	-8.0280350	-1.1157400	2.8995570	89	H	6.7474150	-1.1231930
33	C	-4.9149750	-6.4548950	-2.8716470	90	H	-2.4175110	6.4102400
34	C	3.0844660	7.5002910	2.8656470	91	H	2.4665560	4.3450310
35	C	8.0180090	-1.0770320	-2.9221350	92	H	2.5492040	-4.2524120
36	C	-3.1211600	7.4913650	-2.8696110	93	H	-4.9779070	-0.0613730
37	C	4.2631590	-5.3670600	2.2515230	94	H	-2.5064940	-4.3248490
38	C	-6.7974040	-0.9823960	2.2350880	95	H	4.9605340	-0.0338880
39	C	-4.1957690	-5.4420330	-2.2154030	96	H	-2.5120560	4.3322750
40	C	2.5754550	6.3673430	2.2089890	97	H	3.9185300	-6.0524970
41	C	6.7883160	-0.9465190	-2.2553840	98	H	-7.2269650	-0.3301840
42	C	-2.6048660	6.3609870	-2.2143100	99	H	-3.8426260	-6.1617290
43	C	3.3443690	-4.5750740	2.9788750	100	H	3.3755530	6.4266930
44	C	-5.6520350	-0.5879900	2.9653300	101	H	7.2082560	-0.2969690
45	C	-3.2929260	-4.6409230	-2.9524760	102	H	-3.4305690	6.4105800
46	C	2.3418830	5.1831260	2.9463330	103	N	0.7854550	1.6251470
47	C	5.6401760	-0.5576670	-2.9838600	104	N	1.0104870	-1.4890050
48	C	-2.3723840	5.1761120	-2.9506840	105	N	-1.0057440	-1.5015000
49	C	3.2183470	-4.8339590	4.3635320	106	N	-0.8041180	1.6224320
50	C	-5.8160340	-0.3459810	4.3490380	107	N	1.7945320	-0.1168920
51	C	-3.1640590	-4.9119710	-4.3345540	108	N	-1.8039870	-0.1308480
52	C	2.6410330	5.2090590	4.3284330	109	N	4.8815470	-6.6058340
53	C	5.8007090	-0.3157990	-4.3680690	110	N	-8.1854750	-0.8850310
54	C	-2.6823030	5.1979350	-4.3303880	111	N	-4.7927540	-6.7142400
55	C	3.9975040	-5.8445780	4.9509940	112	N	3.3704410	7.5260070
56	C	-7.0839390	-0.5060650	4.9326780	113	N	8.1718770	-0.8474050
57	C	-3.9247470	-5.9434740	-4.9099660	114	N	-3.4157720	7.5136250
					115	Ru	-0.0046080	0.0016980

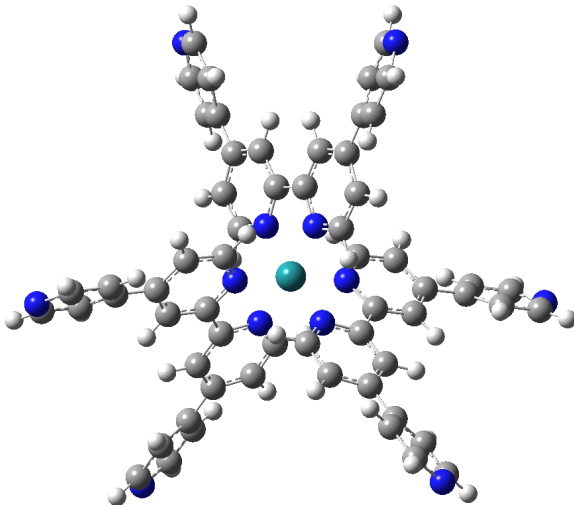
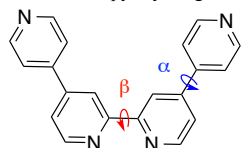


Figure S6: Representation of the optimised geometry of $[Ru(qpy)_3]^{2+}$ (PBE0 / LanL2DZ)

Table S4: Characteristic dimensions of the of $[Ru(qpy)_3]^{2+}$ complex compared to XRD values.

		$[Ru(qpy)_3]^{2+}$	
	DFT value	XRD value Cl salt	XRD value PF_6 salt
N-Ru-N angle ($^{\circ}$)	78.3	77.6(2)	78.79(17)
Ru-N distances (\AA)	2.092	2.052(4)	2.056(4)
			2.052(4)
d_{C-C} between cycles of the 4,4' sites (\AA)	1.487	1.475(8)	1.480(9)
			1.490(8)
d_{C-C} between cycles of the 2,2' site (\AA)	1.478	1.465(10)	1.486(7)
α , average planes* angles ($^{\circ}$) of the 4,4' sites	30.3	28	17
			32
β , average planes* angles ($^{\circ}$) of the 2,2' sites	1.8	0	9

* Average planes were calculated taking the six atoms of a pyridyl ring.



The optimisation of the geometry of the complex shows a distorted octahedral coordination sphere for the metal centre with angles formed by ligands and metallic centre of approximately 78° . The quaterpyridine presents a classic average planes angle of the pendant pyridines (α) of about 30° and a planarity of the 2,2'-bipyridine site (average planes angle β of 2°). The replacement of the *para* hydrogen of a bpy ligand by a 4-pyridyl substituent does not seem to affect the general geometry of the molecule when compared to $[Ru(bpy)_3]^{2+}$.

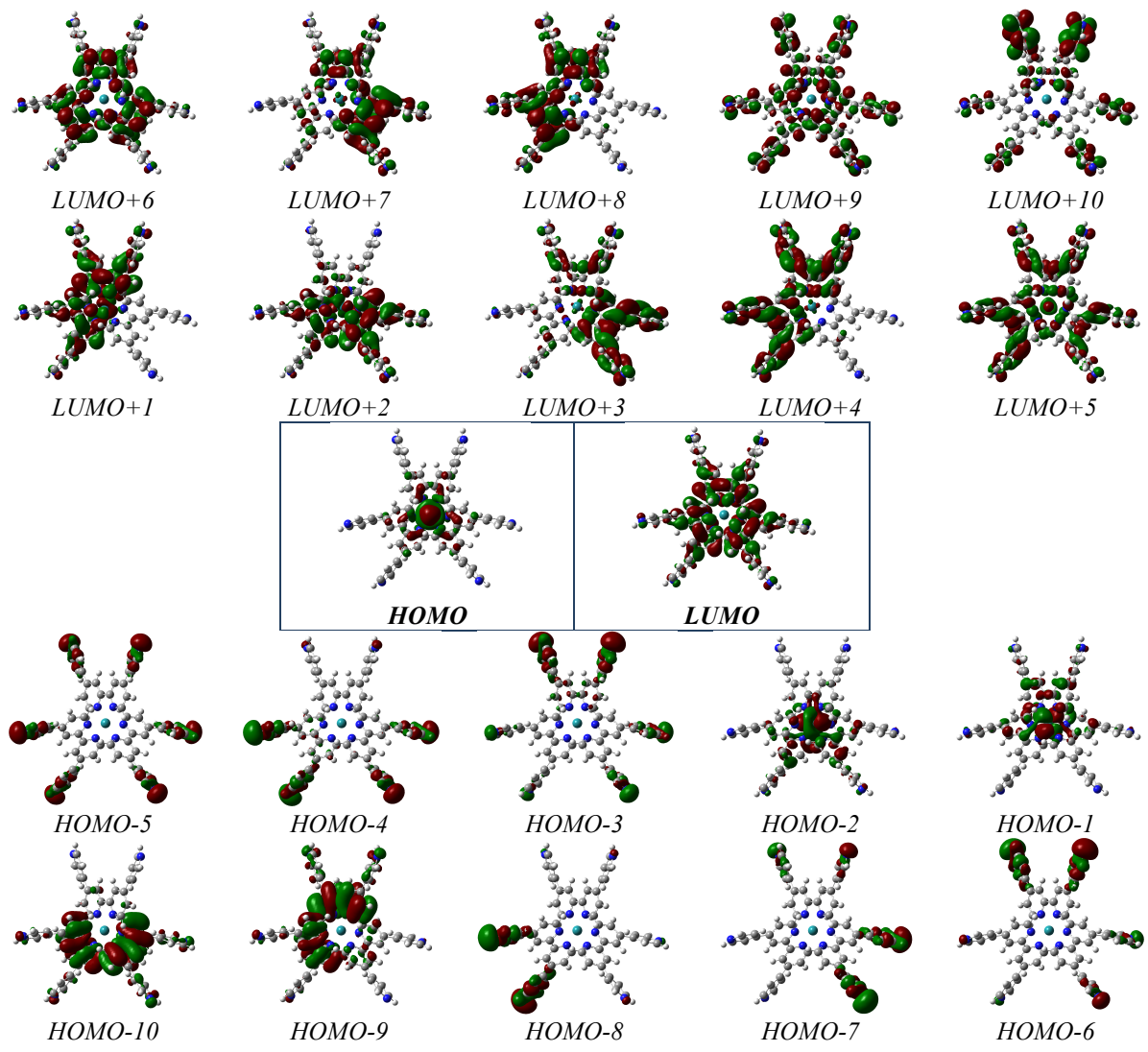


Figure S7 : Representation of the molecular orbitals involved in the vertical electronic transitions computed for $[Ru(qpy)_3]^{2+}$.

Table S5: Calculated Vertical Excited States of $[Ru(qpy)_3]^{2+}$ (E: energy, λ : wavelength, O.S.: Oscillator Strength)

No.	E (cm ⁻¹)	λ (nm)	O.S.	63	36674	272.7	0	126	40979	244.0	0.0134
1	20352	491.4	0.0014	64	36701	272.5	0.0003	127	40986	244.0	0.0008
2	20362	491.1	0.0017	65	36705	272.4	0.0002	128	40989	244.0	0.0737
3	20462	488.7	0.0177	66	37028	270.1	0.0457	129	40992	244.0	0.0686
4	21580	463.4	0.0052	67	37032	270.0	0.0474	130	41032	243.7	0.0102
5	21922	456.2	0.0443	68	37140	269.2	0	131	41035	243.7	0.0106
6	21940	455.8	0.0486	69	37262	268.4	0.0013	132	41073	243.5	0.0113
7	22735	439.8	0.3082	70	37268	268.3	0.0015	133	41094	243.3	0.0001
8	22748	439.6	0.315	71	37321	267.9	0.0001	134	41099	243.3	0.0002
9	24828	402.8	0	72	37393	267.4	0	135	41107	243.3	0.0002
10	27637	361.8	0.0255	73	37428	267.2	0.0084	136	41398	241.6	0.2086
11	27794	359.8	0.1223	74	37434	267.1	0.0085	137	41400	241.5	0.0092
12	27804	359.7	0.1243	75	37557	266.3	0.0002	138	41407	241.5	0.0072
13	28557	350.2	0.0002	76	37711	265.2	0.1229	139	41437	241.3	0.0171
14	28687	348.6	0.1917	77	37715	265.1	0.1195	140	41445	241.3	0.0144
15	28688	348.6	0.1926	78	37749	264.9	0.0045	141	41456	241.2	0.152
16	28878	346.3	0.0042	79	38191	261.8	0	142	41477	241.1	0.0005
17	28882	346.2	0.0033	80	38268	261.3	0.0001	143	41489	241.0	0.0007
18	29013	344.7	0.1718	81	38270	261.3	0.0001	144	41491	241.0	0.0004
19	29021	344.6	0.0394	82	38296	261.1	0.0003	145	41813	239.2	0.0089
20	29025	344.5	0.0017	83	38300	261.1	0.0007	146	41817	239.1	0.0117
21	29771	335.9	0.0357	84	38301	261.1	0.0051	147	41834	239.0	0.0224
22	29776	335.8	0.0354	85	38327	260.9	0.0041	148	41854	238.9	0.003
23	29902	334.4	0	86	38722	258.3	0.002	149	41855	238.9	0.001
24	30844	324.2	0.0053	87	38735	258.2	0.0015	150	41859	238.9	0.0009
25	30850	324.1	0.0052	88	38812	257.6	0	151	41868	238.8	0.0172
26	31094	321.6	0	89	38913	257.0	0.002	152	41872	238.8	0.0083
27	31301	319.5	0.0273	90	38917	257.0	0.0001	153	41882	238.8	0.1069
28	31304	319.4	0.0271	91	38920	256.9	0	154	41946	238.4	0.0001
29	32170	310.9	0.0004	92	38931	256.9	0.0003	155	41986	238.2	0.0011
30	32311	309.5	0.0365	93	38943	256.8	0	156	41997	238.1	0.0009
31	32319	309.4	0.0357	94	38952	256.7	0	157	42056	237.8	0.053
32	32334	309.3	0.0216	95	38958	256.7	0	158	42080	237.6	0.0001
33	32360	309.0	0.0005	96	39229	254.9	0.231	159	42094	237.6	0.0044
34	32372	308.9	0.0014	97	39233	254.9	0.2291	160	42096	237.6	0.0041
35	32380	308.8	0.0017	98	39309	254.4	0.0057	161	42158	237.2	0.0179
36	32621	306.6	0	99	39316	254.4	0.0067	162	42159	237.2	0.0173
37	34126	293.0	0.243	100	39574	252.7	0.0006	163	42184	237.1	0.0008
38	34134	293.0	0.246	101	39575	252.7	0.0004	164	42186	237.0	0.0013
39	34514	289.7	0.9151	102	39718	251.8	0	165	42286	236.5	0.193
40	35086	285.0	0.112	103	39749	251.6	0	166	42303	236.4	0.1299
41	35108	284.8	0.1084	104	39758	251.5	0.0001	167	42308	236.4	0.1273
42	35224	283.9	0.0682	105	40062	249.6	0.2341	168	42504	235.3	0.0559
43	35505	281.7	0	106	40068	249.6	0.2294	169	42509	235.2	0.0562
44	35639	280.6	0.0004	107	40241	248.5	0.0002	170	42573	234.9	0.0108
45	35648	280.5	0.0003	108	40376	247.7	0.1659	171	42732	234.0	0.0001
46	35798	279.3	0.0001	109	40376	247.7	0.1673	172	42746	233.9	0.0229
47	35807	279.3	0.0001	110	40402	247.5	0.227	173	42748	233.9	0.0229
48	35822	279.2	0.0002	111	40512	246.8	0.0344	174	42831	233.5	0.0902
49	36003	277.8	0.0219	112	40514	246.8	0.0241	175	42834	233.5	0.0743
50	36015	277.7	0.0222	113	40519	246.8	0.0098	176	42837	233.4	0.0704
51	36053	277.4	0.0062	114	40533	246.7	0	177	42857	233.3	0.0013
52	36067	277.3	0.0065	115	40535	246.7	0.0004	178	42887	233.2	0.09
53	36069	277.2	0.0162	116	40601	246.3	0.0064	179	42888	233.2	0.0891
54	36069	277.2	0.0159	117	40611	246.2	0.0136	180	43011	232.5	0.0004
55	36088	277.1	0.0039	118	40612	246.2	0.0126	181	43013	232.5	0.0009
56	36097	277.0	0.0013	119	40657	246.0	0.0538	182	43014	232.5	0.0014
57	36117	276.9	0.1731	120	40860	244.7	0.0036	183	43039	232.3	0.0011
58	36237	276.0	0.0033	121	40868	244.7	0.029	184	43040	232.3	0.0012
59	36246	275.9	0.0033	122	40874	244.7	0.0242	185	43115	231.9	0.1029
60	36486	274.1	0.0001	123	40878	244.6	0.0037	186	43174	231.6	0.0002
61	36497	274.0	0.0001	124	40889	244.6	0.0018	187	43199	231.5	0.0028
62	36501	274.0	0.0001	125	40938	244.3	0.047	188	43203	231.5	0.0017

189	43204	231.5	0.0094	227	44252	226.0	0.0004	265	46854	213.4	0.0054
190	43211	231.4	0.0104	228	44259	225.9	0.0004	266	46878	213.3	0.0043
191	43223	231.4	0.0149	229	44441	225.0	0.0009	267	47038	212.6	0.0008
192	43230	231.3	0.0032	230	44445	225.0	0.0008	268	47079	212.4	0
193	43282	231.0	0.0001	231	44508	224.7	0.0064	269	47187	211.9	0.0115
194	43288	231.0	0.0004	232	44810	223.2	0	270	47190	211.9	0.0116
195	43296	231.0	0.0008	233	45087	221.8	0.0154	271	47291	211.5	0.0005
196	43303	230.9	0.0007	234	45095	221.8	0.015	272	47303	211.4	0.0056
197	43304	230.9	0.0008	235	45106	221.7	0.0011	273	47310	211.4	0.0057
198	43353	230.7	0.0005	236	45231	221.1	0.0001	274	47375	211.1	0.0003
199	43353	230.7	0.0005	237	45237	221.1	0.0001	275	47377	211.1	0.0003
200	43366	230.6	0	238	45246	221.0	0.0001	276	47404	211.0	0.0002
201	43370	230.6	0.0002	239	45268	220.9	0.0022	277	47446	210.8	0.0078
202	43465	230.1	0.0001	240	45272	220.9	0.0031	278	47451	210.7	0.0013
203	43512	229.8	0.008	241	45278	220.9	0.0039	279	47452	210.7	0.0089
204	43516	229.8	0.008	242	45310	220.7	0.0116	280	47496	210.5	0.0005
205	43599	229.4	0.0004	243	45322	220.6	0.0112	281	47508	210.5	0.0008
206	43605	229.3	0.0008	244	45374	220.4	0.0001	282	47570	210.2	0
207	43731	228.7	0.0001	245	45377	220.4	0	283	47754	209.4	0.0002
208	43736	228.6	0	246	45405	220.2	0.0008	284	47934	208.6	0.0173
209	43737	228.6	0.0001	247	45751	218.6	0.004	285	47939	208.6	0.0183
210	43745	228.6	0.0001	248	45871	218.0	0	286	47960	208.5	0.0019
211	43749	228.6	0	249	45880	218.0	0	287	47963	208.5	0.0031
212	43751	228.6	0.0001	250	45997	217.4	0.03	288	48065	208.1	0.0001
213	43762	228.5	0	251	46001	217.4	0.0293	289	48074	208.0	0.0001
214	43814	228.2	0.0011	252	46013	217.3	0.0008	290	48134	207.8	0.0268
215	43824	228.2	0.0001	253	46109	216.9	0.0089	291	48331	206.9	0.0003
216	43827	228.2	0.0001	254	46117	216.8	0.0083	292	48375	206.7	0
217	43980	227.4	0.0122	255	46256	216.2	0.0006	293	48382	206.7	0
218	44107	226.7	0	256	46260	216.2	0.0006	294	48566	205.9	0
219	44124	226.6	0.0001	257	46265	216.1	0.0001	295	49214	203.2	0.0004
220	44133	226.6	0.0001	258	46293	216.0	0.0002	296	49232	203.1	0.0004
221	44135	226.6	0	259	46296	216.0	0.0009	297	49479	202.1	0
222	44143	226.5	0.0001	260	46297	216.0	0.0009	298	49624	201.5	0.009
223	44145	226.5	0.0001	261	46329	215.8	0.0001	299	49628	201.5	0.013
224	44147	226.5	0	262	46424	215.4	0.0258	300	49632	201.5	0.0159
225	44174	226.4	0.0002	263	46428	215.4	0.0261				
226	44180	226.3	0.0003	264	46729	214.0	0				

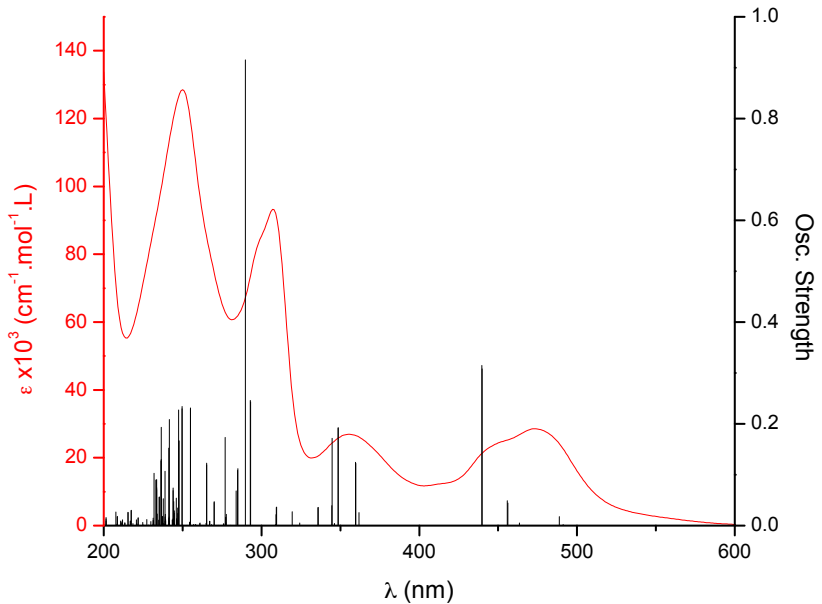


Figure S8: Experimental absorption spectrum (in red) and vertical electronic transitions (in black) computed for $[Ru(qpy)_3]^{2+}$.

The absorption spectrum of $[Ru(qpy)_3]^{2+}$ was measured in acetonitrile and presents four major bands. Time-Dependent Density Functional Theory (TD-DFT) was used to attribute each band to a particular transition. For $[Ru(qpy)_3]^{2+}$, calculations allow the band at $\lambda = 473$ nm and the shoulder around 448 nm to be attributed to a first metal-to-ligand charge-transfer (MLCT), being the superimposition of transitions from HOMO -1 and -2 (primarily metal-based orbitals), to LUMO +1 and +2 (primarily ligand-centred orbitals). Similarly, the band at 356 nm is also attributed to a second MLCT transition absent in $[Ru(bpy)_3]^{2+}$. The band at 307 nm is attributed to a ligand centred transition (LC). Finally, the band at 250 nm corresponds to the last MLCT transition. The major contributions of the orbitals for the most significant transitions with oscillator strengths superior to 0.05 can be found in the next section (*Table S6*). One should notice that the PBE0 functional, while providing the correct excitation energies is not able to fully reproduce their relative intensity. This behaviour has already been noticed in the literature in the case of even simpler compounds and different functionals and more expensive approaches have been used in cases where the band shape is of interest,^{S10} which was actually not the case of the present study.

Table S6 : Orbitals major contributions of significant transitions for [Ru(qpy)₃]²⁺ (oscillator strength superior to 0,05)

No.	λ (nm)	Major contributions
7	439.84	H-2->L+1 (18%), H-2->L+2 (24%), H-1->L+1 (25%), H-1->L+2 (18%)
8	439.59	H-2->L+1 (24%), H-2->L+2 (18%), H-1->L+1 (18%), H-1->L+2 (25%)
11	359.79	HOMO->L+3 (92%)
12	359.66	HOMO->L+4 (92%)
14	348.59	H-2->L+5 (12%), H-1->L+5 (80%)
15	348.58	H-2->L+5 (80%), H-1->L+5 (11%)
18	344.68	H-2->L+3 (36%), H-1->L+3 (40%), H-1->L+4 (15%)
37	293.04	H-10->LUMO (45%), H-9->LUMO (12%)
38	292.96	H-10->LUMO (12%), H-9->LUMO (44%)
39	289.73	H-11->LUMO (50%), H-10->L+2 (10%), H-9->L+1 (10%)
40	285.01	H-10->L+1 (11%), H-9->LUMO (10%), H-9->L+2 (10%), H-3->LUMO (14%)
41	284.84	H-11->L+2 (10%), H-10->LUMO (10%), H-9->L+1 (13%), H-4->LUMO (13%)
42	283.90	H-11->LUMO (11%), H-10->L+2 (19%), H-9->L+1 (11%), H-5->LUMO (27%), H-4->L+2 (11%)
57	276.88	H-17->LUMO (46%), H-16->L+1 (11%), H-15->L+1 (12%)
76	265.18	H-20->L+1 (23%), H-19->L+1 (11%), H-18->L+2 (10%)
77	265.15	H-20->L+2 (22%), H-18->L+1 (16%)
96	254.91	HOMO->L+10 (16%)
97	254.88	H-23->LUMO (10%), HOMO->L+11 (16%)
105	249.61	H-9->L+5 (11%), HOMO->L+10 (25%)
106	249.57	H-10->L+5 (11%), HOMO->L+11 (25%)
108	247.67	H-10->L+6 (21%)
109	247.67	H-9->L+6 (21%)
110	247.51	H-14->L+3 (11%), H-13->L+4 (11%), H-12->L+5 (13%)
119	245.96	H-23->L+1 (19%), H-22->L+2 (20%), H-5->L+6 (24%)
128	243.97	H-16->L+6 (3%), H-14->L+5 (2%), H-10->L+6 (8%), H-9->L+6 (4%), H-4->L+4 (2%), H-4->L+6 (3%), H-3->L+6 (7%),
129	243.95	H-15->L+6 (3%), H-13->L+5 (2%), H-12->L+4 (2%), H-10->L+6 (3%), H-9->L+6 (7%), H-8->L+4 (2%), H-4->L+6
136	241.56	H-11->L+6 (24%), H-6->L+5 (15%)
141	241.22	H-11->L+6 (11%), H-6->L+4 (10%), H-6->L+5 (29%)
153	238.76	H-10->L+4 (19%), H-9->L+3 (11%)
157	237.78	HOMO->L+14 (75%), HOMO->L+16 (11%)
165	236.48	H-11->L+6 (23%), H-9->L+8 (10%)
166	236.39	H-18->L+6 (11%), H-9->L+6 (13%)
167	236.36	H-19->L+6 (11%), H-10->L+6 (13%)
168	235.27	H-2->L+13 (12%), H-1->L+12 (12%)
169	235.24	H-2->L+12 (11%), H-1->L+13 (13%), H-1->L+17 (10%)
174	233.48	H-18->L+5 (11%), H-6->L+7 (10%)
175	233.46	H-18->L+5 (13%), H-8->L+8 (10%)
176	233.44	H-19->L+5 (12%)
178	233.17	H-18->L+5 (10%), H-6->L+7 (14%), H-6->L+8 (14%)
179	233.17	H-8->L+8 (13%), H-7->L+7 (22%)
185	231.94	H-2->L+11 (14%), H-2->L+18 (14%), H-1->L+10 (14%), H-1->L+17 (13%)

S.I.-5 Photocatalysed hydrogen production:

For hydrogen evolution measurements, gas chromatograms were recorded using a Perkin Elmer Clarus-480 gas chromatograph (GC) with a TCD detector, argon as the carrier gas, a 7' HayeSep N 60/80 pre-column, a 9' molecular sieve 13x45/60 column, and a 2 mL injection loop. The gas flow was set to 31.5 mL·min⁻¹ when both columns are in-line. Samples solutions were prepared in standard 20 mL headspace vials and placed in a thermostatic bath set at 20 °C. In a total volume of 10 mL the mixtures were studied in degassed DMF containing 10⁻⁴ M of photosensitiser, 1,2·10⁻³ M of catalyst (prepared in a glove box), 1 M of triethanolamine (TEOA) and 0.1 M of HBF₄ (48% in water). They were sealed with a rubber septum, pierced by two stainless steel tubes. The first tube carried a nitrogen flow pre-bubbled in spectrograde solvent and triethanolamine. The flow was set to 10.2(1) mL/min (adjusted with a manual flow controller (Porter, 1000) and referenced with a digital flowmeter (Perkin Elmer FlowMark)). The second tube sent the flow to the GC sample loop and passed through a 2 mL overflow protection vial, then through a 3-way selection valve (Clippard) before being sent to the GC sample loop. A microprocessor (Arduino Uno) coupled with a custom PC interface allowed for timed injections of up to two channels. For calibration of H₂ production rate at a specific nitrogen flow, a syringe pump (New Era Pump) equipped with a gas-tight syringe (SGE) and a 26s gauge needle (Hamilton) was used to bubble different rates of pure hydrogen gas into the sample, to a minimum of 0.5 µL/minute. This gave a linear fit for peak area for H₂ versus the flow rates of H₂. For calibration testing, stock cylinders of known concentration of H₂ in nitrogen replaced the nitrogen flow (inserted at the pre-bubbler, to keep the same vapor matrix). The measured results, independent of flow rate (under same pressure) can be easily converted into a rate of hydrogen following equation 1.

$$(Eq. 1) \quad H_2 \text{ rate } (\mu\text{L}/\text{min}) = [H_2 \text{ standard}] \text{ (ppm)} \times N_2 \text{ flow rate } (\text{L}/\text{min})$$

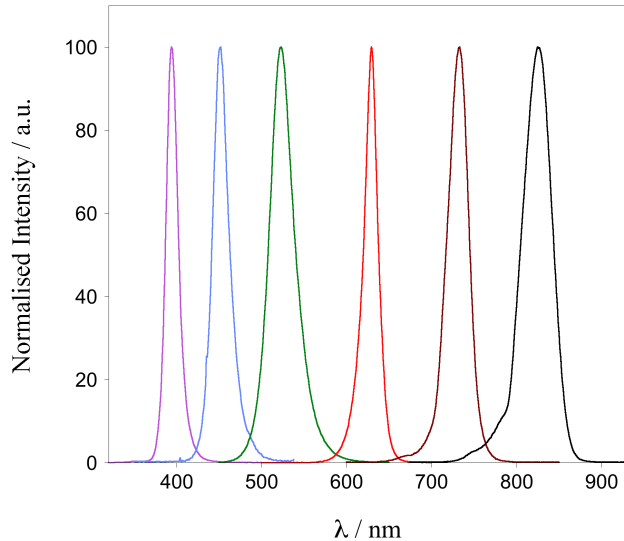


Figure S9: Emission spectra of the lamps used

Table S7 : Emission characteristics of the lamps used

	UV	Blue	Green	Red	Near-IR
λ _{max em.} (nm)	390	460	560	630	730
λ _{max em.} (cm ⁻¹)	25 641	21 739	17 857	15 873	13 699
Δλ (nm)	80	150	170	125	150

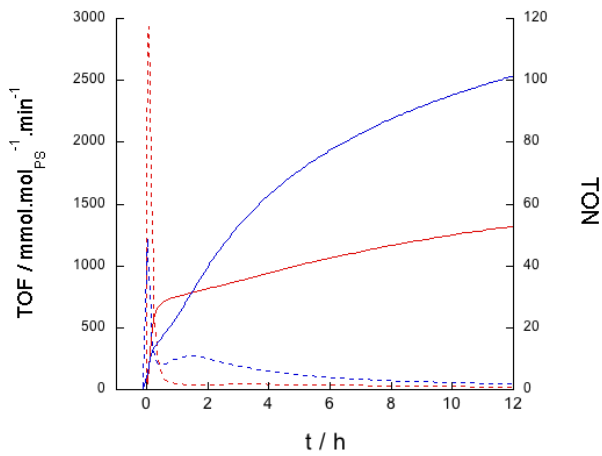


Figure S10 : Photocatalysed hydrogen evolution under blue irradiation of $[Ru(bpy)_3]^{2+}$ (red) and $[Ru(qpy)_3]^{2+}$ (blue). Turn Over Frequencies (dashed line) and Turn Over Number (plain line) are represented, measured in the same conditions.

As depicted in *Figure S10*, $[Ru(bpy)_3]^{2+}$ and $[Ru(qpy)_3]^{2+}$ complexes were studied under blue light irradiation ($\lambda_{\text{max}} = 460$ nm, $\Delta\lambda = \sim 150$ nm as presented in *Figure S9* and *Table S7*) respectively. Both complexes behaved similarly, although $[Ru(qpy)_3]^{2+}$ presents a better general efficiency. No period of induction was noticed after turning on the lamp. $[Ru(qpy)_3]^{2+}$ and $[Ru(bpy)_3]^{2+}$ presents a maximal TOF at the start of 1250 and 3000 $\text{mmol} \cdot \text{mol}_{\text{PS}}^{-1} \cdot \text{min}^{-1}$, respectively. The abrupt decrease observed during the first hour is attributed to a decomposition of the PS as usually described in the literature on Ru/Co systems. The TON of $[Ru(qpy)_3]^{2+}$ finally reach 100 after 12 hours whereas in the same condition $[Ru(bpy)_3]^{2+}$ presents only 55. In both cases, the rate of hydrogen production has not yet reached zero at the end of the experiment, indicating that the low quantity of PS remaining is still active.

In similar experiments, the apparent pH of the medium has been measured roughly equal to 9. The overall experimental conditions are then basic. Given that the pKa of TEOA is 7.74 and the one of the quaterpyridine is 3 in the ground state and 5 in the excited state,^{S11} the protonation of the complex will not occur. However, to confirm it, we measured the absorption spectra of the PS, giving a MLCT transition at 473 nm, then added HBF_4 , red-shifting the MLCT band to 489 nm. The addition of TEOA in the ratio of hydrogen evolution studies, returned the MLCT band back at 473 nm, indicating that the protonation of the PS is not responsible for the red-light driven hydrogen production as compared with $[Ru(bpy)_3]^{2+}$.

References

- S1. G. A. Crosby and J. N. Demas, *J. Phys. Chem.*, 1971, **75**, 991-1024.
- S2. K. Suzuki, A. Kobayashi, S. Kaneko, K. Takehira, T. Yoshihara, H. Ishida, Y. Shiina, S. Oishi and S. Tobita, *Phys. Chem. Chem. Phys.*, 2009, **11**, 9850-9860.
- S3. A. Shi, M. R. Pokhrel and S. H. Bossmann, *Synthesis*, 2007, 505-514.
- S4. E. Duli  re, M. Devillers and J. Marchand-Brynaert, *Organometallics*, 2003, **22**, 804-811.
- S5. K. Chichak and N. R. Branda, *Chem. Commun.*, 2000, 1211-1212.
- S6. M. J. Frisch, G. W. Trucks, H. B. Schlegel, G. E. Scuseria, M. A. Robb, J. R. Cheeseman, G. Scalmani, V. Barone, B. Mennucci, G. A. Petersson, H. Nakatsuji, M. Caricato, X. Li, H. P. Hratchian, A. F. Izmaylov, J. Bloino, G. Zheng, J. L. Sonnenberg, M. Hada, M. Ehara, K. Toyota, R. Fukuda, J. Hasegawa, M. Ishida, T. Nakajima, Y. Honda, O. Kitao, H. Nakai, T. Vreven, J. A. Montgomery Jr., J. E. Peralta, F. Ogliaro, M. J. Bearpark, J. Heyd, E. N. Brothers, K. N. Kudin, V. N. Staroverov, R. Kobayashi, J. Normand, K. Raghavachari, A. P. Rendell, J. C. Burant, S. S. Iyengar, J. Tomasi, M. Cossi, N. Rega, N. J. Millam, M. Klene, J. E. Knox, J. B. Cross, V. Bakken, C. Adamo, J. Jaramillo, R. Gomperts, R. E. Stratmann, O. Yazyev, A. J. Austin, R. Cammi, C. Pomelli, J. W. Ochterski, R. L. Martin, K. Morokuma, V. G. Zakrzewski, G. A. Voth, P. Salvador, J. J. Dannenberg, S. Dapprich, A. D. Daniels,   . Farkas, J. B. Foresman, J. V. Ortiz, J. Cioslowski and D. J. Fox, Gaussian, Inc., Wallingford, CT, USA, 2009.
- S7. C. Adamo and V. Barone, *J. Chem. Phys.*, 1999, **110**, 6158-6170.
- S8. (a) T. H. Dunning Jr and P. J. Hay, *Modern Theoretical Chemistry*, III edn., Plenum, New York, 1977; (b) P. J. Hay and W. R. Wadt, *J. Chem. Phys.*, 1985, **82**, 270-283; (c) P. J. Hay and W. R. Wadt, *J. Chem. Phys.*, 1985, **82**, 299-310; (d) W. R. Wadt and P. J. Hay, *J. Chem. Phys.*, 1985, **82**, 284-298.
- S9. M. Cossi, N. Rega, G. Scalmani and V. Barone, *J. Comput. Chem.*, 2003, **24**, 669-681.
- S10. A. Charaf-Eddin, A. Planchat, B. Mennucci, C. Adamo and D. Jacquemin, *J. Chem. Theory Comput.*, 2013, **9**, 2749-2760.
- S11. A. M. W. Cargill Thompson, M. C. C. Smailes, J. C. Jeffery and M. D. Ward, *J. Chem. Soc., Dalton Trans.*, 1997, 737-744.